Reaching a Double-Digit Dielectric Constant with Fullerene Derivatives

Rousseva, Sylvia; den Besten, Hugo; van Kooij, Felien S.; Doting, Eva L.; Doumon, Nutifafa Y.; Douvogianni, Evgenia; Koster, L. Jan Anton; Hummelen, Jan C.

Published in:
Journal of Physical Chemistry C

DOI:
10.1021/acs.jpcc.0c01390

THE JOURNAL OF PHYSICAL CHEMISTRY C

pubs.acs.org/JPCC

Article

Reaching a Double-Digit Dielectric Constant with Fullerene Derivatives

Sylvia Rousseva, Hugo den Besten, Felien S. van Kooij, Eva L. Doting, Nutifafa Y. Doumon, Evgenia Douvogianni, L. Jan Anton Koster, and Jan C. Hummelen*

Cite This: J. Phys. Chem. C 2020, 124, 8633–8638

Read Online

ACCESS | Metrics & More | Article Recommendations | Supporting Information

ABSTRACT: The dielectric constant (ε_r) of organic semiconductors is a key material parameter for improving device performance in the field of organic electronics. However, the effect of the dielectric constant on the electronic and optoelectronic properties of materials remains unclear due to the scarcity of known organic semiconductors with an ε_r value higher than 6. Herein, the optical and electronic properties of a homologous series of fullerene derivatives with high ε_r are studied. The low frequency (<10^6 Hz) ε_r is extracted from the capacitance measured using impedance spectroscopy, and the effect of length (n) and geometrical arrangement of the polar ethylene glycol (EG) side chains is investigated. The ε_r is found to correlate with length for the symmetrical Bingel adducts, whereas for the unsymmetrical branched-EG chain adducts there is no significant difference between the two EG chain lengths. For BTrEG-2, the ε_r reaches 10, which is an unprecedented value in monoadduct fullerene derivatives. These materials open up new possibilities of studying the effect of ε_r in organic electronic devices such as organic photovoltaics, organic thermoelectrics, and organic field-effect transistors.

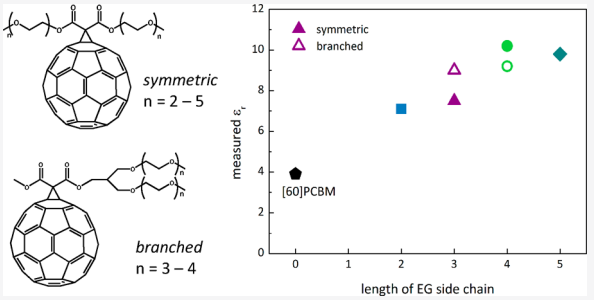

INTRODUCTION

Organic semiconductors have great potential as a class of materials for electronic applications, due to their large variety of possible and tunable properties, such as flexibility, biodegradability, and solution processability. The tunability through structural design allows widespread applicability and has led to the development of different "design rules" depending on the target electronic device, whether it be organic light-emitting diodes (OLEDs), organic field-effect transistors (OFETs), organic thermoelectrics (OTEs), or organic photovoltaics (OPVs).

One main difference between organic and inorganic semiconductors lies in their dielectric properties. In most presently known organic semiconductors, the relative dielectric constant (ε_r) is low ($\varepsilon_r \approx 3-4$) and as a result, charges in the material are poorly screened and experience relatively strong Coulombic forces.[1] This can have a profound effect on charge transport, recombination kinetics, and device performance.[2] For instance, at high carrier densities such as found in OFETs, simulations suggest that Coulomb interactions between charge carriers significantly reduce their mobility.[3] Meanwhile, in doped organic semiconductors, the low permittivity leads to the formation of Coulomb traps that decrease their effective conductivity.[4] In organic photovoltaics, the low ε_r is particularly significant as it brings about the formation of bound electron–hole pairs, similar to localized Frenkel excitons.[5] This hinders the separation of photogenerated electrons and holes, limiting the power conversion efficiencies that can be obtained in working devices comprising one active semiconductor.

Recently, tailoring the dielectric constant of organic semiconductors has gained attention after being proposed as a design strategy for high-efficiency OPVs by Koster et al.[6] In their theoretical study, the authors showed that increasing the permittivity of organic semiconductors in a model bulk heterojunction (BHJ) device could largely alleviate many of the problems of OPV devices by lowering the exciton binding energy and reducing both geminate and nongeminate recombination losses.[6] Furthermore, an ε_r of 10 could theoretically lower the exciton binding energy to below k_bT (~25 meV), effectively allowing for the generation of free charge carriers in an organic semiconductor at room temperature. Further theoretical work illustrated that polar side chains which increase the ε_r, can lower the Coulomb attraction and stabilize charge-separated states.[7,8]

Efforts to increase the ε_r of organic semiconductors synthetically have focused on adding polar groups to known

Received: February 18, 2020
Revised: March 18, 2020
Published: April 2, 2020

conjugated organic materials.[9] Reorientation of the dipoles in the presence of an electric field increases ε_r in the low-frequency regime, (<10^6 Hz) and by incorporating these groups in side chains, the dielectric properties can be tuned while leaving the core structure of the material unchanged. Ethylene glycol (EG) chains have been shown to be a particularly apt choice, due to the low barriers for rotation, which allows for flexibility of the chain even in the solid state.[10,11] The flexibility also improves $\pi-\pi$ stacking which is beneficial for charge carrier mobility in thin films.[12] A range of polymers,[10,13−15] small molecules,[16−18] and fullerene derivatives[19] with EG side chains showing increased ε_r have been reported.

Experimentally, the role of the increased ε_r of these glycolated organic semiconductors in working devices remains vaguely understood. In one case, the addition of EG chains to [60]PCBM (Figure 1) led to higher recombination rates in

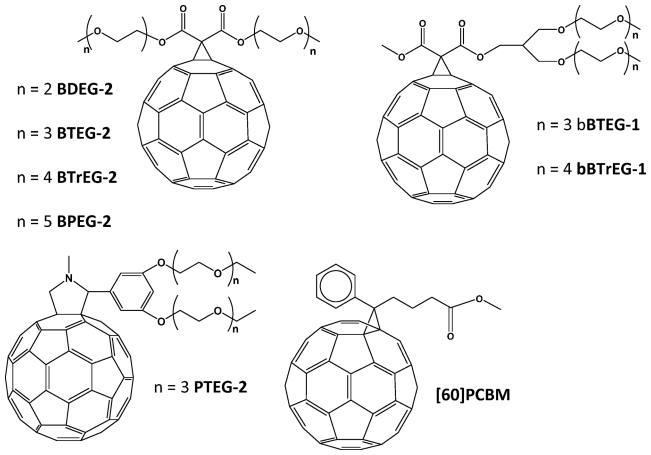

Figure 1. Structure of the new (top row) and previously reported (bottom row) fullerene derivatives studied in this work.

bulk heterojunction solar cells, which was attributed to the increased amount of trap states.[20] Furthermore, the time scales of dielectric response required to affect the performance of organic materials in a device are still under debate.[21] However, some initial studies show promising results. Recently Armin et al.[22] and Liu et al.[17] reported higher values for the static dielectric constant of two glycolated small molecule acceptors and investigated single semiconductor OPV devices. Both groups found external quantum efficiencies (EQE) of 4−5% for these devices, whereas the EQE response of the reference alkylated materials was negligible, showing that the enhanced dielectric constant of the active layer has an effect on charge extraction.

Furthermore, Liu et al. recently showed that in organic thermoelectric devices, the electrostatic interactions between the host material and dopant have an effect on the doping efficiency and conductivity of fullerene films doped with n-DMBI.[23] They found that for PTEG-1 (ε_r = 5.7) the doping efficiency was higher and that the activation energy for charge generation was lower than for [60]PCBM (ε_r = 4). They postulated that the charge transfer complexes between host and dopant formed during the doping process were more likely to dissociate due to interactions between the polar environment created by the EG chain around the fullerene and the charge-transfer complex.

However, a thorough investigation of the potential of high ε_r organic semiconductors in OPV, organic thermoelectrics, and other electronic devices remains limited by the rarity of materials with ε_r surpassing 6 in the solid state. Furthermore, side-chain geometry can often have a profound effect on device performance, but its effect on the ε_r of fullerene derivatives remains unclear. Inspired by our previous work[11,19] we continued our investigation of fullerene adducts with polar side chains. We focus on fullerene derivatives as they are an interesting class of molecules, with good charge carrier mobilities and potential uses not only in OPVs but also as electron-transporting layers in hybrid perovskite[24] and other types of PV cells, and as materials for n-type thermoelectric devices.[25]

In this work, we report on a homologous series of Bingel adducts of C_{60} having an increasing number of EG units in the side chains. We also vary the geometry by making two unsymmetrical adducts containing branched EG chains. We find that for the symmetrical adducts, the low frequency ε_r increases with chain length, reaching ε_r = 10.2 for BTrEG-2 (n = 4) after which the value appears to saturate. In contrast, for the branched EG chains we did not see a clear difference when the chain length was increased. To the best of our knowledge, this is the highest dielectric constant measured to date for monoadduct fullerene derivatives, and the value close to 10 has significant implications for the nature of excitons in the film. Aware of the challenges involved in measuring the ε_r of organic materials with impedance spectroscopy,[26,27] we have taken rigorous steps to ensure correct and accurate measurements and interpretations in order to obtain solid ε_r values for the intrinsic (undoped) semiconductor materials (details in the Supporting Information).

EXPERIMENTAL DETAILS

General. The synthesis of the Bingel adducts studied in this work is described in the Supporting Information. PTEG-2 was synthesized according to a previously reported procedure.[19] [60]PCBM was purchased from Solenne BV and used without further purification.

Device Fabrication. Commercially available glass substrates patterned with indium−tin−oxide (ITO) were used for all capacitors, and standard 3 cm × 3 cm glass substrates were used for the electron-only devices. The substrates were scrubbed with soapy water, rinsed with deionized water, sonicated in acetone and isopropyl alcohol, spin dried, further dried in an oven at 140 °C for 10 min, and subjected to 20 min of UV−ozone treatment before use. PEDOT:PSS water solution (Clevios P VP AI4083) was filtered through PTFE filters (0.45 μm), spin-cast in ambient conditions, and annealed in the oven at 140 °C for 10 min. All fullerene derivatives were spin-cast from anhydrous solutions under N_2 atmosphere in the glovebox. Aluminum top/bottom electrodes and LiF/Ca were deposited by thermal evaporation at a pressure less than 10^{-6} mbar.

Film Characterization. Device thicknesses were measured using a DEKTAK 6 M Stylus Profiler and taken as an average from different locations on the substrate area. AFM images were captured in ScanAsyst mode using a Bruker MultiMode AFM-2 with Scanasyst-Air tips. Impedance measurements were carried out under N_2 atmosphere in the dark using a Solartron 1260 impedance gain-phase analyzer and an AC drive voltage of 10−15 mV. For the variable-temperature measurements, the N_2 flow into the substrate holder was cooled using liquid

https://dx.doi.org/10.1021/acs.jpcc.0c01390
J. Phys. Chem. C 2020, 124, 8633−8638

Table 1. Properties of the Fullerene Derivatives and [60]PCBM Given as Reference

material	$E_{red}^{1/2}$ **1**[a]	$E_{red}^{1/2}$ **2**[a]	estimated LUMO level [eV][b]	μ_e [$cm^2V^{-1}s^{-1}$][c]	ε_r[d] (10–10^6 Hz)	ε_r at 10^4 Hz
[60]PCBM	−1.11	−1.50	−3.69	1.0×10^{-3}	3.9 ± 0.1[18]	
BDEG-2	−1.08	−1.46	−3.72	1.8×10^{-3}	7.1 (0.4, 15 devices)	6.4 (0.4)
BTEG-2	−1.08	−1.46	−3.72	2.1×10^{-3}	7.5 (0.8, 20 devices)	7.2 (0.4)
BTrEG-2	−1.10	−1.45	−3.70	1.1×10^{-4}	10.2 (0.8, 16 devices)	9.3 (0.7)
BPEG-2	−1.09	−1.46	−3.71	1.0×10^{-4}	9.8 (0.6, 20 devices)	9.2 (0.5)
bBTEG-1	−1.04	−1.44	−3.76	6.5×10^{-3}	9.0 (0.6, 7 devices)	8.5 (0.9)
bBTrEG-1	−1.06	−1.45	−3.74	8.4×10^{-4}	9.2 (0.3, 8 devices)	8.4 (0.7)

[a]In V, measured relative to ferrocene Fc/Fc+. [b]Estimated relative to the ferrocene standard using the formula $-(E_{red}^{1/2} + 4.8)$ eV. [c]Measured using the SCLC method (see Supporting Information). [d]The ε_r is given as the average value of the devices measured with the standard deviation and the number of devices measured given in brackets. The ε_r at 10^4 Hz follows the same trend as the average.

nitrogen, and the temperature was monitored using a thermocouple. The temperature stability was ±1–2 degrees throughout the measurement. The current–voltage (J–V) curves for the single carrier devices were measured under N_2 atmosphere in a glovebox in the dark using a Keithley 2400 source meter.

RESULTS AND DISCUSSION

Synthesis. The symmetrical series of fullerene adducts (Figure 1) with varying lengths of EG chains were synthesized in two steps (Scheme S1). First, the esterification of malonic acid with the desired length EG-monomethyl ether was carried out under Steglich conditions using EDCI (*N*-(3-(dimethylamino)propyl)-*N*′-ethylcarbodiimide hydrochloride) as the coupling reagent and DMAP (4-(dimethyl amino)-pyridine) as the catalyst. The resulting malonic esters were reacted with C_{60} via the Bingel reaction to afford the four fullerene derivatives (B1–B4) in yields of 49–52%. The esterification was also attempted using DCC (dicyclohexylcarbodiimide) but this was unsuccessful under a variety of conditions. For BPEG-2 (B4) some problems were encountered with the precipitation, as the solid was very sticky and it was not possible to transfer the product without dissolving it. For fullerenes derivatives B5 and B6 (Figure 1), the synthesis of the asymmetrical malonate was achieved in four steps: starting with the synthesis of the branched EG chain, according to the literature procedure,[14] then esterification of the unsymmetrical malonic acid monomethyl ester obtained by hydrolysis of dimethyl malonate[28] (Scheme S2). This was then reacted with C_{60} under the same conditions for fullerene derivatives B1–4.

Material Characterization. The structures of BDEG-2, BTEG-2, BTrEG-2, BPEG-2, bBTEG-1, and bBTrEG-1 were confirmed by $^1H/^{13}C$ NMR spectroscopy, FT-IR spectroscopy, and high-resolution mass spectrometry (see Supporting Information). The signal of the sp^3 hybridized carbon directly attached to the C_{60} in the Bingel adducts was very weak in the ^{13}C NMR spectra. However, we were able to locate it at ∼52 ppm by measuring on a 600 MHz instrument. The highly symmetrical character of derivatives B1–B4 is confirmed by the few signals (14 peaks in the aromatic region) seen for the fullerene carbon atoms. In contrast, for the branched derivatives, the symmetry is reduced and two peaks were seen corresponding to the different carbonyl carbons and 26 peaks for the fullerene carbon atoms. All four derivatives are highly polar and showed an enhanced solubility in a variety of solvents compared to C_{60} and [60]PCBM. The enhanced solubility in more polar solvents is welcomed as it opens up the possibility of fabricating devices from green solvents.

UV–vis absorption spectra in chloroform solutions show the typical absorption characteristics of fullerene Bingel adducts. (Figure S1) The lowest energy transition can be seen as a weak absorption peak at 687–688 nm. The low intensity of this band arises from the symmetry forbidden nature of this low energy transition in fullerene derivatives.[27] In the spin-cast films the absorption spectrum is broadened and loses sharp features and the onset of absorption is red-shifted. No significant difference is seen in the absorption characteristics within the series. (Figure S1). The electrochemical properties were studied in solution using cyclic voltammetry (Figure S2). The first and second half-wave reduction potentials were determined by measurements in 1 mM solutions relative to ferrocene (Table 1). All derivatives showed the characteristic three reduction peaks of the fullerene cage seen for [60]PCBM as well. The lowest unoccupied molecular orbital (LUMO) level was estimated by using ferrocene as an internal standard. The shifts in the LUMO level within the series were small.

Impedance Spectroscopy. The low-frequency dielectric constant of the symmetrical fullerene derivatives was measured using impedance spectroscopy. Parallel plate-type capacitors with the device structure glass/ITO/PEDOT:PSS/fullerene/aluminum were fabricated. Apart from PEDOT:PSS, which serves as a hole transport and planarization layer at the ITO electrode, other interlayers were omitted to prevent any effects of bulk doping caused by interlayer migration which could undermine the validity of the measured dielectric properties.[29] The fullerene-derivatives were spin-cast from several solvents (chloroform, ODCB, chlorobenzene, and THF). Spin-casting from chlorobenzene generally gave the best results for uniform film coverage of the substrate. The surface roughness, a crucial parameter in the accurate determination of ε_r from "parallel plate" capacitors, was quantified from atomic force microscopy (AFM) images of the film surface morphology (Figures S3–S4, Table S1).[30]

The impedance was measured over the frequency range 1–10^6 Hz at constant DC bias, and the capacitance was obtained by equivalent circuit fitting. (Figure S8) After measuring the thickness, the apparent ε_r could then be obtained. We then calculated the roughness parameters and the roughness correction factor.[30] (Figure S7, Tables S1). In our case, the calculated RMS roughnesses were small, and the roughness correction factor was close to one for all films (Table S1). For this reason we chose not to apply the correction and to use the raw capacitance results. The final values, taken as the average of the devices measured with the standard deviation as the error, for each compound were 7.1 ± 0.4 (15 devices), 7.5 ± 0.8 (20 devices), 10.2 ± 0.8 (16 devices), and 9.8 ± 0.6 (20 devices) for BDEG-2, BTEG-2, BTrEG-2, and BPEG-2,

https://dx.doi.org/10.1021/acs.jpcc.0c01390
J. Phys. Chem. C 2020, 124, 8633–8638

respectively (Table 1, Figure 2). We note that the standard deviation gives an idea of the spread of the values measured

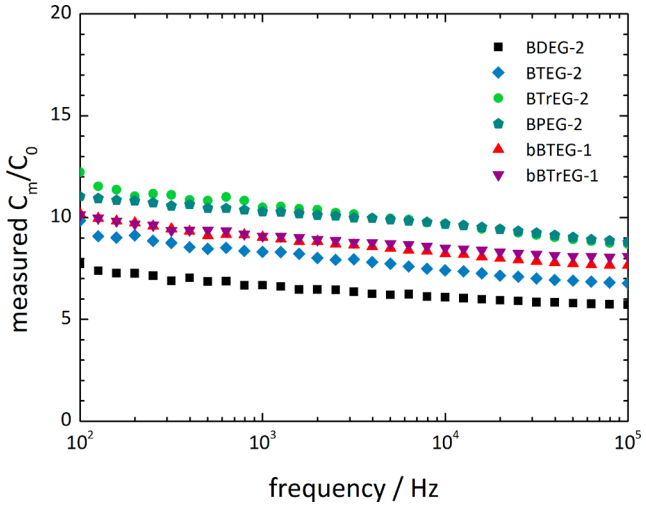

Figure 2. Dielectric constant vs frequency for one representative device of each of the Bingel adducts investigated in this work, measured at 295 K, at 0 V DC bias.

which arises due to variations in the quality of spin-cast films and errors in the measurement of the thickness, the capacitance, and the fitting model used.

In Figure 2, it can be seen that the capacitance increased gradually at frequencies below 10^4 Hz for all four Bingel adducts, leading to a variable dielectric constant across the frequency range measured. Furthermore, as can be seen in the capacitance vs frequency graphs, (Figures S10–S13) the equivalent circuit fitting gives an average value across the frequency range and does not fit the data well at lower frequencies when the capacitance increases. For this reason we report the ε_r at 10^4 Hz alongside the average values in Table 1. One hypothesis is that this may be due to co-operative movement/reorientation of the permanent dipoles in the EG side chains becoming more probable at longer time scales. To gain further insight, the impedance of BTEG-2 was measured at different temperatures. The movement of the EG chains should be hindered at lower temperatures as rotation about the bonds is a thermally activated process with an energy barrier.[11]

As can be seen in Figure 3 the slope of the capacitance vs frequency graph is reduced dramatically when the measurement is carried out at 200 K. [60]PCBM and PTEG-2 (see Figure 1 for structure) were also measured for comparison. In the case of [60]PCBM, the changes in the spectra upon cooling were very small. Since this molecule contains only one relatively inflexible permanent dipole (the carbonyl group), the larger part of the contribution to the capacitance is attributed to the electronic polarization of the delocalized π electrons of the fullerene cage which occurs at optical frequencies ($\sim 10^{12}$ Hz) and is unaffected by changes in temperature. In contrast, PTEG-2 also shows distinct changes to the capacitance as the temperature is decreased. This suggests that the EG chains are not only contributing to the capacitance increase at lower frequencies for the Bingel adducts, but also for other fullerene derivatives. The difference in the temperature range measured is much greater in the case of the Bingel adducts than with PTEG-2, which may suggest higher flexibility of the side chains in the film. Further investigations into the cause of this frequency dependence are currently ongoing in our lab.

Another reason for the increase in capacitance at lower frequencies may be "unintentional doping" arising from impurities in the material from the synthesis and/or purification steps or from reactive interlayers used in the device stack. To test this, capacitance–voltage measurements were carried out at fixed frequencies (Figure S16). A Mott–Schottky plot[27,31] of the data did not show a clear straight-line region at forward bias from which we could extract a doping density. The capacitance remains stable until the applied voltage exceeds the built-in voltage and the device begins to conduct (Figure S16). For this reason, we conclude that no significant doping effects are present and that the measured dielectric constant values are intrinsic to the material.

Seeing as the ε_r of the Bingel adducts was much higher than our previously measured fullerene derivatives PTEG-1 and PTEG-2,[19] we speculated that the orientation of the EG chains, in this case extending in two directions, may affect the packing and hence flexibility of the dipoles at room temperature under an applied electric field. As a more direct comparison, the asymmetric fullerene Bingel adducts bBTEG-1 and bBTrEG-1 were synthesized and investigated. The same device structure and measurement methods were used to measure the dielectric constant, giving final values of 9.0 ± 0.6 (8 devices) and 9.2 ± 0.3 (7 devices) (Table S2, Figures S14

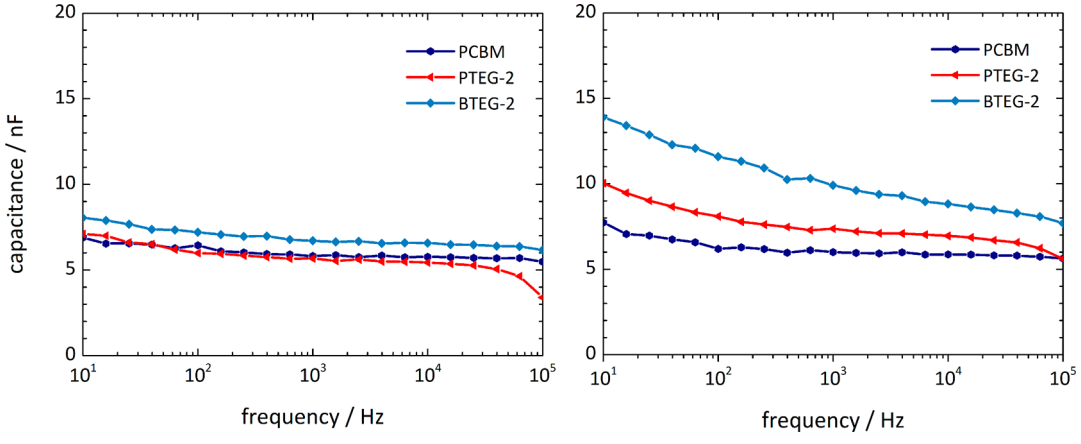

Figure 3. Capacitance vs frequency plots for three different fullerene derivatives with (PTEG-2 and BTEG-2) and without ([60]PCBM) TEG chains at 200 K (left) and 280 K (right), measured at 0 V DC bias and an applied AC voltage of 15 mV.

https://dx.doi.org/10.1021/acs.jpcc.0c01390
J. Phys. Chem. C 2020, 124, 8633–8638

and S15). In contrast to the symmetrical adducts, no distinct difference in the measured ε_r was seen when increasing the length of the branched chain from n = 3 to 4. Furthermore, the problem of pinholes arose in the spin-cast films, which may be due to the amphiphilic nature of the asymmetric adducts. (Figure S4)

These results show that increasing the length of the EG chain in the symmetrical Bingel adducts leads to an increase in the dielectric constant until n = 4, with BTrEG-2 having the highest dielectric constant of all fullerene derivatives measured in our group to date.[19,32] At even longer chain lengths, the ε_r saturates, and it becomes difficult to work with the material. For the branched Bingel adducts, the ε_r is still high but does not show a clear dependence on length for the two different side-chain lengths studied.

Charge Carrier Mobility. To check if the electronic properties of the fullerene films are affected by the side chains, the electron mobility was measured using the space charge limited current technique (SCLC). The $J-V$ curves of single carrier devices were fitted with the Murgatroyd equation according to the protocol developed by Blakesley et al.[33] We found that the Bingel adducts with EG chain lengths of four or larger exhibited electron mobilities around an order of magnitude lower than the Bingel adducts with the shorter EG side chains and the reference compound, [60]PCBM (Table 1). This suggests that when increasing the ε_r using side-chain engineering, it is important to find the right ratio between flexible polar side chains (EG) and the semiconductor "backbone" (fullerene) to maintain high charge carrier mobility in the film. Nevertheless, the electron mobility is still within the range typically measured for fullerene derivatives and other OSCs using the SCLC method (10^{-3}–10^{-5} cm^2 V^{-1} s^{-1}).

CONCLUSIONS

We have synthesized a series of fullerene derivatives with increasing lengths of oligoethylene glycol chains via the Bingel reaction. The low frequency dielectric constant was measured, and we found that for the symmetrical derivatives, the value correlates with chain lengths up until n = 4, after which the ε_r saturates. In contrast, for the unsymmetrical derivatives, bBTEG-1 and bBTrEG-1, there is no clear difference when increasing the chain length from n = 3 to 4. All six fullerene derivatives have a high ε_r with BTrEG-2 having an average ε_r of 10.2 ± 0.8 which is more than twice that of the reference compound [60]PCBM. Furthermore, with this compound we have for the first time achieved the synthesis and measurement of a fullerene-based semiconductor material with a double-digit dielectric constant. This property has important implications for the nature of excitons and polarons in the material, and we look forward to using these high ε_r molecular semiconductors in furthering our understanding of increased permittivity in organic electronic devices including solar cells and organic thermoelectrics.

ASSOCIATED CONTENT

Supporting Information

The Supporting Information is available free of charge at https://pubs.acs.org/doi/10.1021/acs.jpcc.0c01390.

^{1}H and ^{13}C NMR spectra, UV–vis spectra in solution and film, cyclic voltammograms, Nyquist and Bode plots, $C-V$ plots, AFM images, and the $J-V$ curves from the single carrier devices (PDF)

AUTHOR INFORMATION

Corresponding Author

Jan C. Hummelen − *Stratingh Institute for Chemistry and Zernike Institute for Advanced Materials, University of Groningen, Groningen 9747 AG, The Netherlands;* Email: j.c.hummelen@rug.nl

Authors

Sylvia Rousseva − *Stratingh Institute for Chemistry and Zernike Institute for Advanced Materials, University of Groningen, Groningen 9747 AG, The Netherlands;* orcid.org/0000-0001-9774-3641

Hugo den Besten − *Stratingh Institute for Chemistry and Zernike Institute for Advanced Materials, University of Groningen, Groningen 9747 AG, The Netherlands*

Felien S. van Kooij − *Stratingh Institute for Chemistry and Zernike Institute for Advanced Materials, University of Groningen, Groningen 9747 AG, The Netherlands*

Eva L. Doting − *Stratingh Institute for Chemistry and Zernike Institute for Advanced Materials, University of Groningen, Groningen 9747 AG, The Netherlands*

Nutifafa Y. Doumon − *Zernike Institute for Advanced Materials, University of Groningen, Groningen 9747 AG, The Netherlands;* orcid.org/0000-0002-2625-1647

Evgenia Douvogianni − *Stratingh Institute for Chemistry and Zernike Institute for Advanced Materials, University of Groningen, Groningen 9747 AG, The Netherlands*

L. Jan Anton Koster − *Zernike Institute for Advanced Materials, University of Groningen, Groningen 9747 AG, The Netherlands;* orcid.org/0000-0002-6558-5295

Complete contact information is available at: https://pubs.acs.org/10.1021/acs.jpcc.0c01390

Notes

The authors declare no competing financial interest.

ACKNOWLEDGMENTS

This work is part of the research program of the Foundation for Fundamental Research on Matter (FOM), which is part of The Netherlands Organization for Scientific Research (NWO). This is a publication by the FOM Focus Group 'Next Generation Organic Photovoltaics', participating in the Dutch Institute for Fundamental Energy Research (DIFFER). N.Y.D. was supported by the Zernike Incentive Bonus Scheme Grant. The authors acknowledge A. F. Kamp and T. Zaharia for their technical assistance with the equipment in the clean room and measurement lab.

REFERENCES

(1) Nelson, J. Polymer: Fullerene Bulk Heterojunction Solar Cells. *Mater. Today* **2011**, *14*, 462–470.

(2) Clarke, T. M.; Durrant, J. R. Charge Photogeneration in Organic Solar Cells. *Chem. Rev.* **2010**, *110*, 6736–6767.

(3) Liu, F.; Van Eersel, H.; Xu, B.; Wilbers, J. G. E.; De Jong, M. P.; Van Der Wiel, W. G.; Bobbert, P. A.; Coehoorn, R. Effect of Coulomb Correlation on Charge Transport in Disordered Organic Semiconductors. *Phys. Rev. B: Condens. Matter Mater. Phys.* **2017**, *96*, 1–8.

(4) Arkhipov, V. I.; Emelianova, E. V.; Heremans, P.; Bässler, H. Analytic Model of Carrier Mobility in Doped Disordered Organic Semiconductors. *Phys. Rev. B: Condens. Matter Mater. Phys.* **2005**, *72*, 2–6.

(5) Zhu, L.; Yi, Y.; Wei, Z. Exciton Binding Energies of Nonfullerene Small Molecule Acceptors: Implication for Exciton Dissociation

Driving Forces in Organic Solar Cells. *J. Phys. Chem. C* **2018**, *122*, 22309−22316.
(6) Koster, L. J. A.; Shaheen, S. E.; Hummelen, J. C. Pathways to a New Effi Ciency Regime for Organic Solar Cells. *Adv. Energy Mater.* **2012**, *2*, 1246−1253.
(7) De Gier, H. D.; Broer, R.; Havenith, R. W. A. Non-Innocent Side-Chains with Dipole Moments in Organic Solar Cells Improve Charge Separation. *Phys. Chem. Chem. Phys.* **2014**, *16*, 12454−12461.
(8) Kraner, S.; Scholz, R.; Koerner, C.; Leo, K. Design Proposals for Organic Materials Exhibiting a Low Exciton Binding Energy. *J. Phys. Chem. C* **2015**, *119*, 22820−22825.
(9) Brebels, J.; Manca, J. V.; Lutsen, L.; Vanderzande, D.; Maes, W. High Dielectric Constant Conjugated Materials for Organic Photovoltaics. *J. Mater. Chem. A* **2017**, *5*, 24037−24050.
(10) Breselge, M.; Van Severen, I.; Lutsen, L.; Adriaensens, P.; Manca, J.; Vanderzande, D.; Cleij, T. Comparison of the Electrical Characteristics of Four 2,5-Substituted Poly(p-Phenylene Vinylene) Derivatives with Different Side Chains. *Thin Solid Films* **2006**, *511*−*512*, 328−332.
(11) Torabi, S.; Jahani, F.; Van Severen, I.; Kanimozhi, C.; Patil, S.; Havenith, R. W. A.; Chiechi, R. C.; Lutsen, L.; Vanderzande, D. J. M.; Cleij, T. J.; Hummelen, J. C.; Koster, L. J. A. Strategy for Enhancing the Dielectric Constant of Organic Semiconductors Without Sacrificing Charge Carrier Mobility and Solubility. *Adv. Funct. Mater.* **2015**, *25*, 150−157.
(12) Meng, B.; Song, H.; Chen, X.; Xie, Z.; Liu, J.; Wang, L. Replacing Alkyl with Oligo(Ethylene Glycol) as Side Chains of Conjugated Polymers for Close π-π Stacking. *Macromolecules* **2015**, *48*, 4357−4363.
(13) Brebels, J.; Douvogianni, E.; Devisscher, D.; Thiruvallur Eachambadi, R.; Manca, J.; Lutsen, L.; Vanderzande, D.; Hummelen, J. C.; Maes, W. An Effective Strategy to Enhance the Dielectric Constant of Organic Semiconductors-CPDTTPD-Based Low Bandgap Polymers Bearing Oligo(Ethylene Glycol) Side Chains. *J. Mater. Chem. C* **2018**, *6*, 500−511.
(14) Chen, X.; Zhang, Z.; Ding, Z.; Liu, J.; Wang, L. Diketopyrrolopyrrole-Based Conjugated Polymers Bearing Branched Oligo(Ethylene Glycol) Side Chains for Photovoltaic Devices. *Angew. Chem., Int. Ed.* **2016**, *55*, 10376−10380.
(15) Meng, B.; Liu, J.; Wang, L. Oligo(Ethylene Glycol) as Side Chains of Conjugated Polymers for Optoelectronic Applications. *Polym. Chem.* **2020**, *11*, 1261−1270.
(16) Donaghey, J. E.; Armin, A.; Burn, P. L.; Meredith, P. Dielectric Constant Enhancement of Non-Fullerene Acceptors via Side-Chain Modification. *Chem. Commun.* **2015**, *51*, 14115−14118.
(17) Liu, X.; Xie, B.; Duan, C.; Wang, Z.; Fan, B.; Zhang, K.; Lin, B.; Colberts, F. J. M.; Ma, W.; Janssen, R. A. J.; Huang, F.; Cao, Y. A High Dielectric Constant Non-Fullerene Acceptor for Efficient Bulk-Heterojunction Organic Solar Cells. *J. Mater. Chem. A* **2018**, *6*, 395−403.
(18) Jang, B.; Lee, C.; Lee, Y. W.; Kim, D.; Uddin, M. A.; Kim, F. S.; Kim, B. J.; Woo, H. Y. A High Dielectric N-Type Small Molecular Acceptor Containing Oligoethyleneglycol Side-Chains for Organic Solar Cells. *Chin. J. Chem.* **2018**, *36*, 199−205.
(19) Jahani, F.; Torabi, S.; Chiechi, R. C.; Koster, L. J. A.; Hummelen, J. C. Fullerene Derivatives with Increased Dielectric Constants. *Chem. Commun.* **2014**, *50*, 10645−10647.
(20) Hughes, M. P.; Rosenthal, K. D.; Dasari, R. R.; Luginbuhl, B. R.; Yurash, B.; Marder, S. R.; Nguyen, T. Q. Charge Recombination Dynamics in Organic Photovoltaic Systems with Enhanced Dielectric Constant. *Adv. Funct. Mater.* **2019**, *29*, 1−8.
(21) Sami, S.; Haase, P. A. B.; Alessandri, R.; Broer, R.; Havenith, R. W. A. Can the Dielectric Constant of Fullerene Derivatives Be Enhanced by Side-Chain Manipulation? A Predictive First-Principles Computational Study. *J. Phys. Chem. A* **2018**, *122*, 3919−3926.
(22) Armin, A.; Stoltzfus, D. M.; Donaghey, J. E.; Clulow, A. J.; Nagiri, R. C. R.; Burn, P. L.; Gentle, I. R.; Meredith, P. Engineering Dielectric Constants in Organic Semiconductors. *J. Mater. Chem. C* **2017**, *5*, 3736−3747.
(23) Liu, J.; Shi, Y.; Dong, J.; Nugraha, M. I.; Qiu, X.; Su, M.; Chiechi, R. C.; Baran, D.; Portale, G.; Guo, X.; Koster, L. J. A. Overcoming Coulomb Interaction Improves Free-Charge Generation and Thermoelectric Properties for n-Doped Conjugated Polymers. *ACS Energy Lett.* **2019**, *4*, 1556−1564.
(24) Castro, E.; Murillo, J.; Fernandez-Delgado, O.; Echegoyen, L. Progress in Fullerene-Based Hybrid Perovskite Solar Cells. *J. Mater. Chem. C* **2018**, *6*, 2635−2651.
(25) Zhang, Q.; Sun, Y.; Xu, W.; Zhu, D. Organic Thermoelectric Materials: Emerging Green Energy Materials Converting Heat to Electricity Directly and Efficiently. *Adv. Mater.* **2014**, *26*, 6829−6851.
(26) Hughes, M. P.; Rosenthal, K. D.; Ran, N. A.; Seifrid, M.; Bazan, G. C.; Nguyen, T.-Q. Determining the Dielectric Constants of Organic Photovoltaic Materials Using Impedance Spectroscopy. *Adv. Funct. Mater.* **2018**, *28*, 1801542−1801553.
(27) Von Hauff, E. Impedance Spectroscopy for Emerging Photovoltaics. *J. Phys. Chem. C* **2019**, *123*, 11329−11346.
(28) Niwayama, S.; Cho, H.; Lin, C. Highly Efficient Selective Monohydrolysis of Dialkyl Malonates and Their Derivatives. *Tetrahedron Lett.* **2008**, *49*, 4434−4436.
(29) Torabi, S.; Liu, J.; Gordiichuk, P.; Herrmann, A.; Qiu, L.; Jahani, F.; Hummelen, J. C.; Koster, L. J. A. Deposition of LiF onto Films of Fullerene Derivatives Leads to Bulk Doping. *ACS Appl. Mater. Interfaces* **2016**, *8*, 22623−22628.
(30) Torabi, S.; Cherry, M.; Duijnstee, E. A.; Le Corre, V. M.; Qiu, L.; Hummelen, J. C.; Palasantzas, G.; Koster, L. J. A. Rough Electrode Creates Excess Capacitance in Thin-Film Capacitors. *ACS Appl. Mater. Interfaces* **2017**, *9*, 27290−27297.
(31) Kirchartz, T.; Gong, W.; Hawks, S. A.; Agostinelli, T.; Mackenzie, R. C. I.; Yang, Y.; Nelson, J. Sensitivity of the Mott − Schottky Analysis in Organic Solar Cells. *J. Phys. Chem. C* **2012**, *116*, 7672−7680.
(32) Douvogianni, E.; Qiu, X.; Qiu, L.; Jahani, F.; Kooistra, F. B.; Hummelen, J. C.; Chiechi, R. C. Soft Nondamaging Contacts Formed from Eutectic Ga-In for the Accurate Determination of Dielectric Constants of Organic Materials. *Chem. Mater.* **2018**, *30*, 5527−5533.
(33) Blakesley, J. C.; Castro, F. A.; Kylberg, W.; Dibb, G. F. A.; Arantes, C.; Valaski, R.; Cremona, M.; Kim, J. S.; Kim, J. S. Towards Reliable Charge-Mobility Benchmark Measurements for Organic Semiconductors. *Org. Electron.* **2014**, *15*, 1263−1272.

https://dx.doi.org/10.1021/acs.jpcc.0c01390
J. Phys. Chem. C 2020, 124, 8633−8638